DOI: 10.3901/CJME.2011.**.***, available online at www.cjmenet.com; www.cjmenet.com.cn

Design and Mechanical Performance Analysis of a New Wheel Propeller

GAO Fudong*, PAN Cunyun, XU Haijun, and ZUO Xiaobo

College of Mechatronic Engineering and Automation, National University of Defense Technology, Changsha 410073, China

Received June 25, 2010; revised September 14, 2010; accepted March, 2011; published electronically March, 2011

Abstract: Nowadays, how to enhance the maneuverability of autonomous underwater vehicles (AUVs) is an important issue in the domain of international navigation in that most AUVs just have a single function of underwater navigation or submarine movement, while the design of thrusters is the key of solving the problem. The multi-moving state autonomous underwater vehicle in this paper can achieve four functions, such as wheels, legs, thrust, and course control depend on the characteristics of spatial deflexion and continual circumgyratetion of the flexible transmission shaft. A new wheel propeller for the multi-moving state autonomous underwater vehicle is presented through analyzing the mechanical characteristics of the ducted propeller and the contracted and loaded tip (CLT) propeller. Then the computational fluid dynamics (CFD) method is used to simulate numerically different propellers open-water performance by using the Reynolds-averaged Navier-Stokes (RANS) equations and Reynolds stress model (RSM) based on sub-domains hybrid meshes. The predicted thrust coefficients, torque coefficients and pressure of the propellers agree well with the experimental data of their open-water performance. The good consistency shows that the numerical method has good accuracy in the prediction of propeller open-water performance, which guides to design the wheel propeller. Moreover, for the sake of ensuring the security and stability of the AUV when it is moving on the ground, finite element method is used to simulate numerically the intensity and vibration characteristics. The proposed final wheel propeller D4-70 (WPD4-70) has preferable open-water performance and intensity characteristics, which can realize the agile maneuverability of the multi-moving state autonomous underwater vehicle.

Key words: wheel propeller, numerical calculation, computational fluid dynamics, finite element method

1 Introduction

Autonomous underwater vehicles (AUVs) are promising vehicle for military and civilian use because they can fulfill many missions, such as assaults, communications, and obviating torpedoes. Nowadays, how to enhance the maneuverability of AUVs is an important issue in the domain of international navigation in that most AUVs just have a single function of underwater navigation or submarine movement. The university of Tianjin has designed an AUV with capabilities of landing and sitting-bottom, which gets ahead[1]. The multi-moving state AUV in this paper makes use of the flexible transmission shaft based on spherical gear as the kinetic source equipment, on the end of which a new wheel propeller is installed[2–3]. The whole equipment can achieve four functions, such as wheels, legs, thrust, and course control depend on the characteristics of spatial deflexion and continual circumgyratetion of the flexible transmission shaft, shown in Fig. 1. So the design and performance analysis of the wheel propeller are the key steps to make the AUV become a more-functional amphibian weapon.

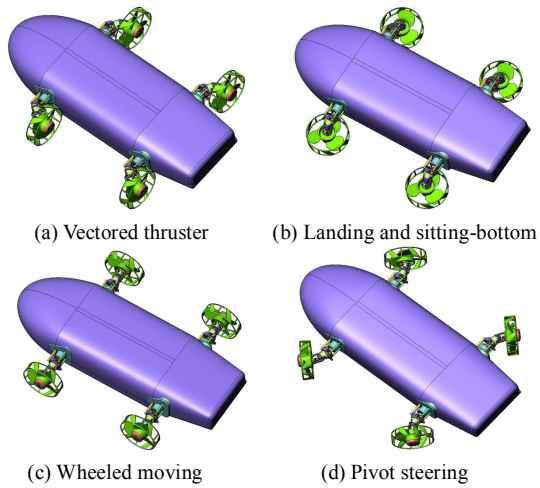

(a) Vectored thruster (b) Landing and sitting-bottom

(c) Wheeled moving (d) Pivot steering

Fig. 1. Typical motions of the AUV

As a thruster in common use, the propellers are of important significance in enhancing the maneuverability and concealment of AUVs through improving its performance. So far, the design of the propeller focuses on two key issues, one is to gain the biggest thrust with limited power, the other is to reduce the vibration and noise for

* Corresponding author. E-mail: gaofudong2005@163.com
This project is supported by National Hi-tech Research and Development Program of China (863 Program, Grant No. 2006AA09Z235), and Hunan Provincial Innovation Foundation For Postgraduate of China (Grant No. B090303)

safety, In order to compute the propellers' performance, some students depend on experiments to get the data, but it still requires sophisticated test facilities and costs tens of thousands of dollars per propeller geometry. Most studies working on design and performance simulation are conducted within the scope of potential flow theory such as lifting surface[4] and panel methods[5] where viscous effect is neglected and flow is assumed to be irrotational. As a method of propeller design, the potential flow theory is used widely, but it is inapplicable to compute propellers' performance in that it can't reveal the characteristics of blade layer, trail of flow field and blade tip vortex flow. Moreover, it neglects the influence of scale effect on performance computation. As the capability of computers has greatly advanced, it is possible to introduce computational fluid dynamics to compute the viscous flow field of propellers, which demonstrates a new way to design propellers.

This paper designs a new wheel propeller according the geometry and flow field of different propellers, which breaks through the traditional design methods. The computational fluid dynamics (CFD) method is used to simulate numerically the propellers' open-water performance by using the RANS equations and RSM based on sub-domains hybrid meshes, which assists to design the wheel propeller. Then the experimental data are used to validate the accurateness of simulation. In addition, in order to ensure the security and stability of the AUV when moving on the ground, finite element method is used to simulate numerically the intensity and vibration characteristics.

2 Mathematical Modeling

2.1 Governing equation

The water is assumed to be incompressible and isothermal Newtonian fluids. The governing equations are written for the mass and momentum conservation, such that

$$\frac{\partial \rho}{\partial t}+\frac{\partial}{\partial x_i}(\rho u_i)=0, \tag{1}$$

$$\frac{\partial}{\partial t}(\rho u_i)+\frac{\partial}{\partial x_j}(\rho u_i u_j)=-\frac{\partial p}{\partial x_i}+\frac{\partial}{\partial x_j}\left[\mu\left(\frac{\partial u_i}{\partial x_j}+\frac{\partial u_j}{\partial x_i}-\frac{2}{3}\delta_{ij}\frac{\partial u_l}{\partial x_l}\right)\right]+\frac{\partial}{\partial x_j}(-\rho\overline{u_i'u_j'})+\rho f_i, \tag{2}$$

where ρ—Density,
t—Time,
u_i, u_j—Velocity in the Cartesian coordinate system,
$\overline{u_i'u_j'}$—Reynolds stresses,
μ—Molecular viscosity,
p—Static pressure,
f_i—Unit mass force,
δ_{ij}—Kronecker delta.

The k-ε, k-w and Reynolds stress model, hereinafter RSM, turbulence models are used for turbulence closure[6–8], which express $-\rho\overline{u_i'u_j'}$ with low-order correlative term or time-average expression. RSM is the most advanced turbulence model for engineering applications and has shown better potential to predict the key features of rotating flows than other models as it bases on turbulence anisotropy and considers the convection and diffuse effect of Reynolds stresses. The RSM can be written in Cartesian tensor form as follows:

$$\begin{aligned}&\frac{\partial}{\partial t}(\rho\overline{u_i'u_j'})+\frac{\partial}{\partial x_k}(\rho u_k\overline{u_i'u_j'})=\frac{\partial}{\partial x_k}\left(\frac{\mu_t}{\sigma_k}\frac{\partial\overline{u_i'u_j'}}{\partial x_k}+\mu\frac{\partial\overline{u_i'u_j'}}{\partial x_k}\right)-\\&\rho\left(\overline{u_i'u_k'}\frac{\partial u_j}{\partial x_k}+\overline{u_j'u_k'}\frac{\partial u_i}{\partial x_k}\right)-C_1\rho\frac{\varepsilon}{k}\left(\overline{u_i'u_k'}-\frac{2}{3}k\delta_{ij}\right)+\\&C_1'\rho\frac{\varepsilon}{k}\left(\overline{u_k'u_m'}n_kn_m\delta_{ij}-\frac{3}{2}\overline{u_i'u_k'}n_jn_k-\frac{3}{2}\overline{u_j'u_k'}n_in_k\right)\frac{k^{3/2}}{C_l\varepsilon d}+\\&C_2'\left(\Phi_{km,2}n_kn_m\delta_{ij}-\frac{3}{2}\Phi_{ik,2}n_jn_k-\frac{3}{2}\Phi_{jk,2}n_in_k\right)\frac{k^{3/2}}{C_l\varepsilon d}-\\&C_2\left(P_{ij}-\frac{1}{3}P_{kk}\delta_{ij}\right)-\frac{2}{3}\rho\varepsilon\delta_{ij}-2\rho\Omega_k(\overline{u_j'u_m'}e_{ikm}+\overline{u_i'u_m'}e_{jkm}),\end{aligned} \tag{3}$$

where k—Turbulence kinetic energy,
ε—Turbulence dissipation rate,
n_k—Element of wall unit normal vector,
d—Distance from study point to fixed wall,
e_{ikm}—Conversion symbol,
Ω_k—Estimate of vortex flow influence,

$$\Phi_{ij,2}=-C_2\left(P_{ij}-\frac{2}{3}P\delta_{ij}\right),$$

$$P_{ij}=-\rho\left(\overline{u_i'u_j'}\frac{\partial u_j}{\partial x_k}+\overline{u_j'u_k'}\frac{\partial u_i}{\partial x_k}\right).$$

C_1=1.8, C_2=0.6, σ_k=0.82, C_l=0.3924, C_μ=0.09, $\mu_t=\rho C_\mu k^2/\varepsilon$, C'_1=0.5, C'_2=0.3.

In order to compute the boundary condition of the Reynolds stress and turbulence dissipation rate, the equations of turbulence kinetic energy k and turbulence dissipation rate ε are determined, which are written as follows:

$$\frac{\partial}{\partial t}(\rho k)(\ )+\frac{\partial}{\partial x_i}(\rho k u_i)=\frac{\partial}{\partial x_j}\left[\left(\mu+\frac{\mu_t}{\sigma_k}\right)\frac{\partial k}{\partial x_j}\right]+\frac{1}{2}P_{ij}-\rho\varepsilon, \tag{4}$$

$$\frac{\partial}{\partial t}(\rho\varepsilon)+\frac{\partial}{\partial x_i}(\rho\varepsilon u_i)=\frac{\partial}{\partial x_j}\left[\left(\mu+\frac{\mu_t}{\sigma_\varepsilon}\right)\frac{\partial\varepsilon}{\partial x_j}\right]+\frac{1}{2}G_{1\varepsilon}P_{ij}-G_{2\varepsilon}\rho\frac{\varepsilon^2}{k}, \tag{5}$$

where $G_{1\varepsilon}$=1.44, $G_{2\varepsilon}$=1.92, σ_k=1.0, σ_ε=1.3.

RSM is a high *Re* turbulence model, which is valid only in fully evolutive turbulence flow. The turbulence fluctuation has more impact than molecular viscosity in the inner region of boundary layer near wall where the turbulence flow is not fully evolutive，so the enhanced wall treatment is adopted in the calculation.

2.2 Numerical method

The computation domain is divided into two regions, one is the inner flow field founded around the propeller, where a revolving coordinate system is fixed on the propeller and tetrahedral cells are filled, the other is the remaining flow field, where a static coordinate system is found and hexahedral cells are filled. Then six layers of prismatic cells are attached to the blade and hub surface with the first spacing off the wall at $y^+\approx1$. The sub-domains hybrid meshes not only adjust the complicated shape of propellers, but also improve the mesh precision and reduce the number. Boundary conditions are set to simulate the flow around a rotating propeller in open water: on the inlet boundary, velocity components of uniform stream with the given inflow speed are imposed; on the exit boundary, the static pressure is set to zero while other variables are extrapolated; on the propeller surface, the no slip condition is imposed; on the outer boundary, the slip boundary condition is imposed, i.e., zero normal velocity component with extrapolated tangential velocity components and static pressure. The mathematics model of flow field is a series of nonlinear equations, which employs a cell-centered finite volume method that allows the adoption of computational elements with arbitrary polyhedral shape. Convection terms are discretized using a second order accurate upwind scheme, while diffusion terms are discretized using a second order accurate central differencing scheme. The velocity-pressure coupling and overall solution procedure are based on a SIMPLE type segregated algorithm. The discretized equations are solved by using pointwise Gauss-Seidel iterations and algebraic multi-grid method which accelerates the solution convergence. The convergence criterion is 0.0001.

3 A New Wheel Propeller Design Procedure

3.1 Numerical validation of a propeller's open-water performance

The propeller model considered in the present study is DTRC3745. This propeller has 5 blades; its diameter is 25.14 cm. The propeller blades have parabolic arc camber and a NACA-16 thickness form. The geometry parameters and offsets for the duct are given in Ref. [9]. HUGHES, et al[9], designed a duct for this propeller by using an existing ducted propeller steady flow (DPSF-2) analysis method, and then the experimental apparatus is used to test the open-water performance of the ducted propeller in a water tunnel. Because the shape of the ducted propeller resembles the wheels, the ducted propeller is chosen to design and study a wheel propeller. The coordinate transformation formula that transforms the local coordinates of the points on section planes to the global coordinates is deduced, the problem of applying different geometric parameter atlases to solid modeling is resolved using the compiled applications. Then the solid modeling is completed with software Solidworks，shown in Fig. 2. The definition of the coordinate axes is: *x* axis is identical with the revolving axis of the propeller with the hub end right direction; *y* axis is identical with the blade reference line; and *z* axis accords with right hand principle.

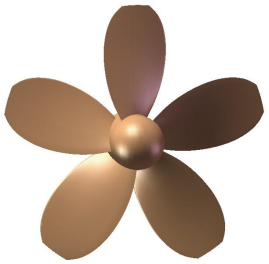

Fig. 2. DTRC3745 propeller geometry

In order to validate the computational method of the propeller's open-water performance, the computational results are compared to the experimental data. The predicted thrust coefficient, torque coefficient and open-water efficiency are in good agreement with the measure values, shown in Fig. 3. The differences with varying advance ratios less than 5.62% and 5.55% for K_t and K_q, respectively, and the discrepancy increases gradually with decreasing propeller load, i.e., increasing *J*. However, K_t results are over-predicted while K_q under-predicted, which result in the predicted open-water coefficient less than experimental data with maximal differences 9.82%. Overall, the agreement is good and the precision is better than that of Refs. [6–7]. It shows that the CFD method in this paper is in good accuracy for the prediction of propeller open-water performance.

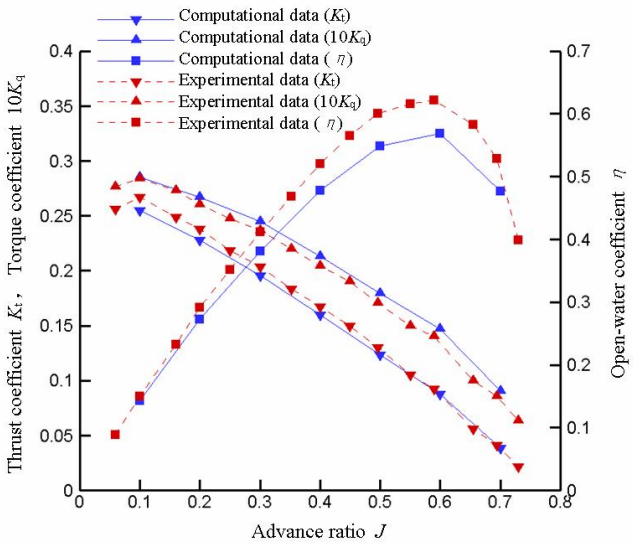

Fig. 3. Computational data and experimental data of DTRC3745's open-water performance

3.2 Compare and analysis of the wheel propeller design scheme

If only consider to realize the wheeled function of the ducted propeller, the ducted propeller with pre-swirl stators or stators behind the propeller can be used as a wheel. However, the flexible transmission shaft can't realize the duct and blades to revolve on different axes, so the duct and blades integrate each other for realizing the wheel function of the propeller. As the duct section is an aerofoil and the duct figure presents the trait of expansion or contractility along the centre axis, the duct's figure needs to be transformed to be columniform for enhancing the intensity and stability when it is used as a wheel, shown in Fig. 4. The improved propeller (model I) realizes the function of wheels, but its hydrodynamic characteristics weaken to a much lower level.

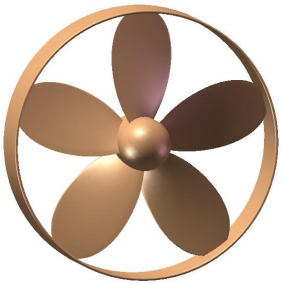

Fig. 4. Model I propeller geometry

Fig. 5 displays the open-water performance curve of model I, which indicates that the thrust decreases, and torque increases compared with DTRC 3745, leading to greatly reduced efficiency. This is mainly due to the combination of duct and blades decrease radial fluid volume, which adds to the pressure loss of pressure side, causing the pressure difference of pressure side and suction side decreases, so the thrust decreases, as shown in Fig. 6. The effect of duct is equivalent to an increase of blade aspect ratio[10], which makes torque increases. The axial and circumferential resistance is also a major influence factor of thrust and torque.

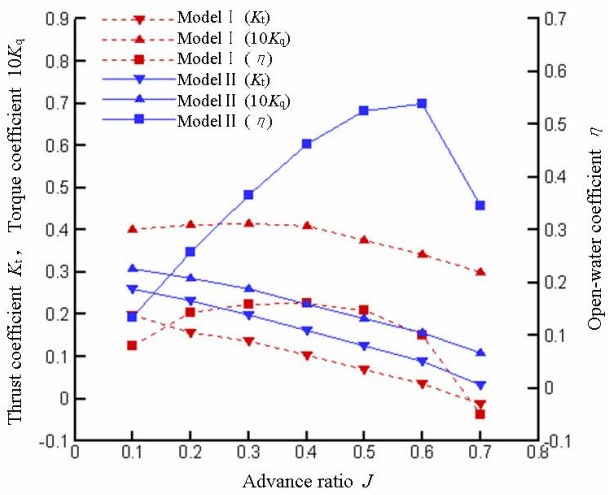

Fig. 5. Open-water performance of model Ⅱ

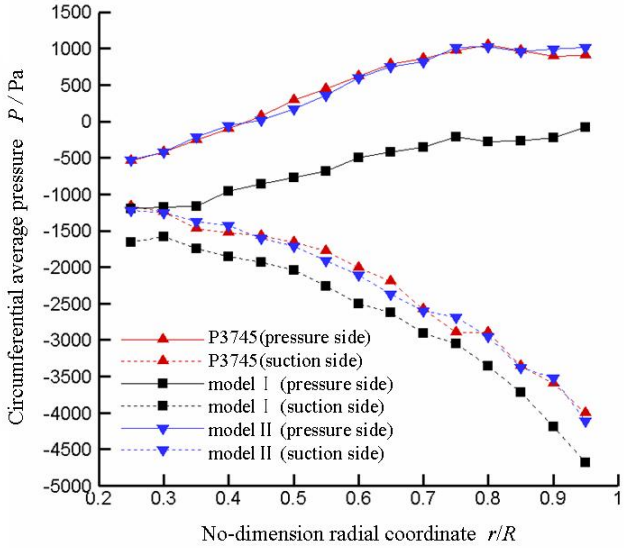

Fig. 6. Circumferential average pressure of different propeller models

To prove the above analysis, retain the tip end plate along the section chord, the remainder of model Ⅰ's duct is removed, as shown in Fig. 7 (model Ⅱ), which is similar to the contracted and loaded tip (CLT) propellers. Currently, CLT propellers have become a focus in international research for its high efficiency, low vibration and not easy to produce cavitation[11]. The CLT propellers have a wide blade tip; an end plate is installed along the direction of the tip section's circle arc so that forms a specific blade circulation on the surface of blades, i.e., the tip vortex maintains a certain degree of intensity and no tip vortex shedding into the wake. Therefore, the blades produce less free vortex strength, which induced smaller loss and higher open-water efficiency than conventional propellers.

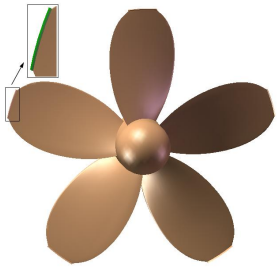

Fig. 7. Model Ⅱ propeller geometry

The open-water performance curve of model Ⅱ is shown in Fig. 5, which has a significant improvement compared with model Ⅰ; the K_t and K_q values increase in similar magnitude compared with DTRC3745, so model Ⅱ puts up the characteristic of high thrust, but there is no improvement of open-water efficiency, which is consistent with experimental conclusion of Ref. [12]. This is because the end plates of CLT propellers are designed to meet wake contraction principle, i.e., it just fit through the flow tube of the propeller disk to reduce the viscous resistance of the end plates. Otherwise, the income of the end plates is lower than the energy consumption of the viscous resistance, so that the open-water efficiency decreases slightly. This is not only to explain why the open-water efficiency of model Ⅰ declines, but also to lay a foundation for the realization of the propeller's wheeled function.

In order to achieve both wheeled function of model Ⅰ and high thrust performance of model Ⅱ, it's important to design a new type of wheel propeller (model Ⅲ) through integrating the advantages of ducted propellers and CLT propellers, shown in Fig. 8. Its open-water performance is obtained by numerical calculation, see Table 1. The hydrodynamic parameters reach the design requirements of a thruster, which are between that of model Ⅰ and model Ⅱ.

Table 1. Computational data of model Ⅲ's open-water performance

Advance ratio J	Thrust coefficient K_t	Torque coefficient $10K_q$	Open-water coefficient η
0.1	0.2372	0.4535	0.0832
0.2	0.2104	0.4442	0.1508
0.3	0.1749	0.4402	0.1897
0.4	0.1368	0.4138	0.2105
0.5	0.0991	0.3898	0.2023
0.6	0.0588	0.3680	0.1526
0.7	0.0024	0.3279	0.0082

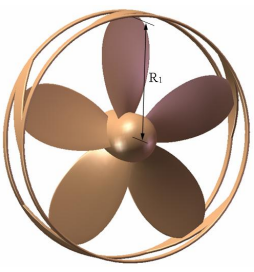

Fig. 8. Model Ⅲ propeller geometry

4 New Wheel Propeller Open-water Performance Analysis

Because of the shortness and thickness of the blade tip chord, the model Ⅲ is prone to stress concentration as a wheel. After further comparative analysis, D-series propellers designed by *China Ship Scientific Research Centre (CSSRC)* are selected to design the ultimate wheel propeller. D-series propellers have no rake but skew, and the blades thickness distribution is nearly equal intensity[13]. The section of the blades adopts Japanese AU_w thickness form at the root and a round profile from $0.6R_2$ to the tip. The chord length of the blade tip section has a certain value and the leading edge and trailing edge have a trait of small round corner. The propeller pitch increases gradually from the root to the tip for deferring the cavitation. The pitch P_x at xR_2 section can be expressed as

$$P_x = P_{0.7}\left(1+\frac{x-0.7}{3}\right). \tag{5}$$

In addition, D-series propellers have a wide advanced coefficient, which can reach 1.4. The high intensity properties and good open-water performance of D-series propellers make it more suitable for wheel propellers design compared with DTRC3745. Based on the D4-70 propeller of this series, a new wheel propeller is designed, see Fig. 9(a). In order to improve the safety factor of intensity, the radius of round ring is reduced to $0.95R_2$, where R_2 is the radius of D4-70 propeller, shown in Fig. 9(b).

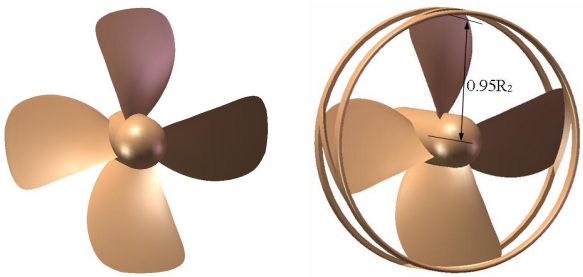

(a) D4-70 propeller geometry (b) Model Ⅳ propeller geometry

Fig. 9. Two propellers geometry

The open-water performance curve of D4-70 propeller is shown in Fig. 10, which indicates that the computational values are in good agreement with the experimental data. Compared with the experimental data, the calculated K_t coefficients with varying advance ratios are slightly less than that of the experiment in general, in the $0.1 \le J \le 0.8$, and the absolute values of relative errors decrease, then increase gradually, the maximum relative error value is 6.85%; while the calculated K_q coefficients with varying advance ratios are slightly less than the experimental data in the $0.1 \le J \le 0.8$, the absolute values of relative errors

decrease gradually and intersect at the J=0.8, then the calculated values are slightly larger than the experimental data and the absolute values of relative errors increase gradually, the maximum relative error value is 5.41%.

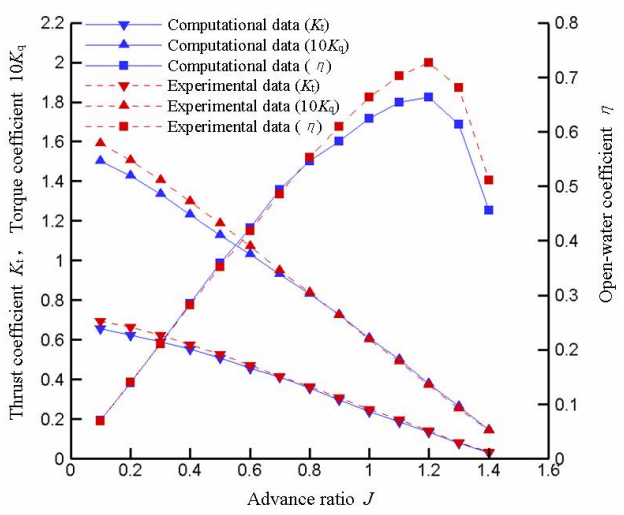

Fig. 10. Computational data and experimental data of D4-70's open-water performance

As for the η-J curve, the computational data and experimental data are in good consistency of $J \leq 0.8$; the relative errors of the computational data and experimental data increase gradually in the $J>0.8$, and the maximum error is 10.92 %, which mainly dues to the reverse error of K_t and K_q at this time. The numerical computation method is further verified by the good precision, which proofs that this method fit to predict the open-water performance of propellers that have different number of leaves, different skewed degrees and different profile forms. It has the potential to replace the propeller model test.

The open-water performance curve of model Ⅳ is shown in Figure 11, compared with the computational results of propeller D4-70, its thrust performance is improved in the $0.1 \leq J \leq 0.8$, then slightly less than it; the calculated K_q with varying advance ratios are slightly more than that of the propeller D4-70 in general, which causes the open-water efficiency of model Ⅳ decrease. As a whole, the propeller model Ⅳ has the characteristics of high thrust, high structural strength, stable hydrodynamic performance and anti-blade flutter, which can meet the design requirements of AUVs' propellers.

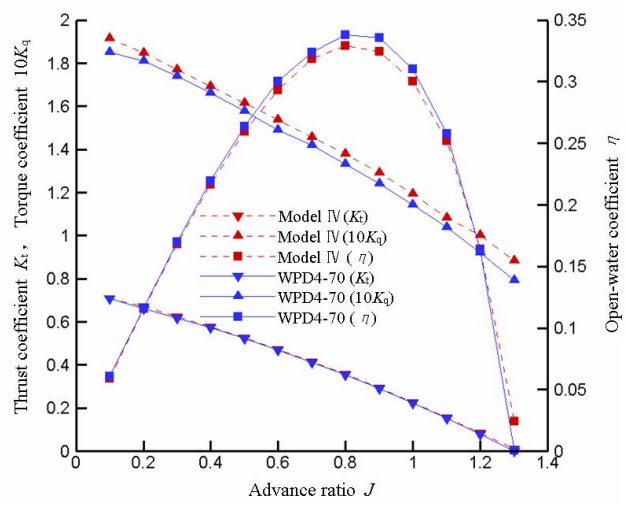

Fig. 11. Open-water performance of model Ⅳ and WPD4-70

To further improve the structural strength of model Ⅳ, the blade maximum thickness of the sections beyond the radius of $0.8R_2$ is increased by 40% and the thickness of the sections within that remains the same, the wheel propeller after some modifications is called WPD4-70 (wheel propeller D4-70), shown in Fig. 12. The computational open-water performance of WPD4-70 shows that: the open-water efficiency of WPD4-70 is very similar with that of model Ⅳ, and has some improvement in the $0.3 \leq J \leq 1.1$, which mainly due to that WPD4-70's torque is slightly smaller than that of model Ⅳ in this range, shown in Fig. 11. Therefore, the structural strength of WPD4-70 is enhanced without lowering open-water performance. In addition, the static pressure distribution of WPD4-70's pressure side is more uniform compared with that of propeller D4-70, shown in Fig. 13, the cavitation and flutter of blades are reduced in advancing process.

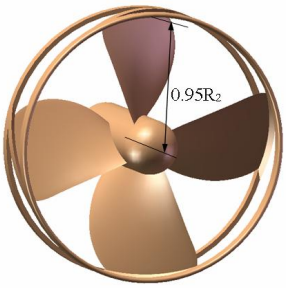

Fig. 12. WPD4-70 propeller geometry

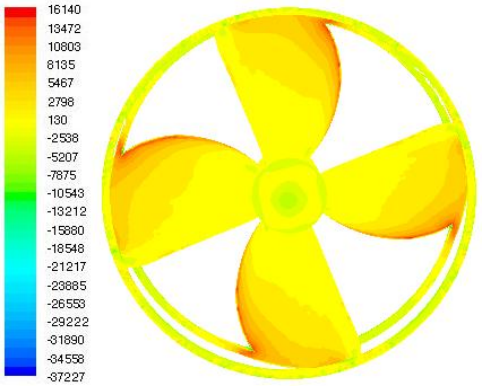

(a) WPD4-70

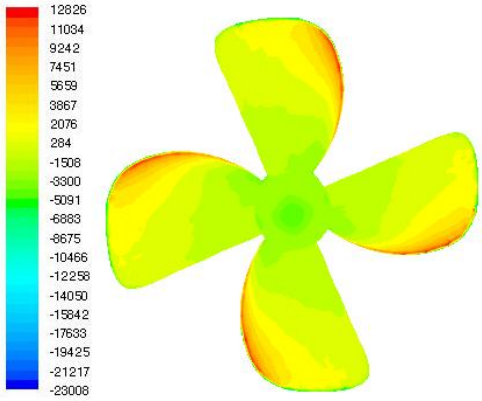

(b) D4-70

Fig. 13. Pressure distribution on the pressure side of WPD4-70 and D4-70 (Pa)

The braking and diving of the AUV navigating in the water are achieved through the propeller reversing. The computational reverse characteristics of WPD4-70 are shown in Fig. 14. The big braking force during speed-down process can realize AUV's urgent brake while the small thrust during speed-up process can ensure its safe landing.

5 New Wheel Propeller Strength Characteristics Analysis

5.1 New wheel propeller nonlinear buckling analysis

The strength characteristic of the wheel propeller is the major factor affecting its stability and safety when the AUV is moving on the ground. As this kind of wheel propeller is a new structure proposed in this paper, there are no related theory applied to analyze the strength characteristic currently, and the experiment not only costs too much but also takes a long time, thus the numerical methods become an effective way to solve the problem[14].

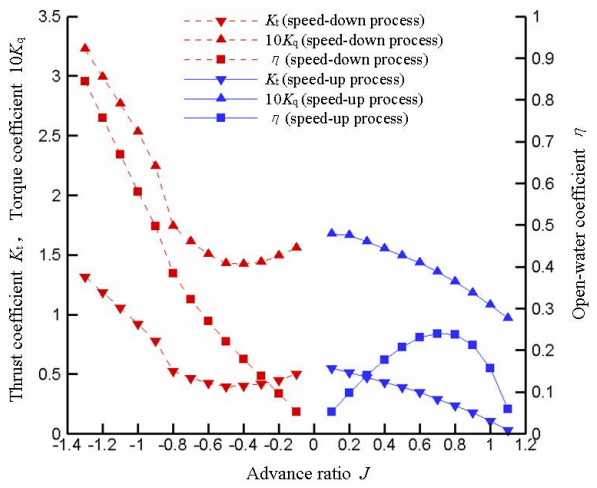

Fig. 14. Open-water performance of WPD4-70's reversion

Establishing a precise finite element model is the precondition of analyzing its strength characteristic, which directly affects the solving accuracy. The material of WPD4-70 is alloy of copper, the elastic modulus E=210 GPa and Poisson's ratio μ=0.28. The body unit SOLID187 is used to mesh WPD4-70 model. According to the geometry and force characteristics of the blades, the regions where the blade thickness varies obviously and exist large concentrated force, such as the root and tip, use the small size mesh, the size of the rest meshes properly increase with uniform transition. Taking into account of the state of the wheel propeller moving on the ground, where name the angle of the line from landing point to the origin and the y-axis θ. The nonlinear buckling analysis of WPD4-70 at θ=0°, θ=45° and the model Ⅳ at θ=45° is made. The relation curve about the load and the maximum displacement of nodes is obtained, shown in Fig. 15.

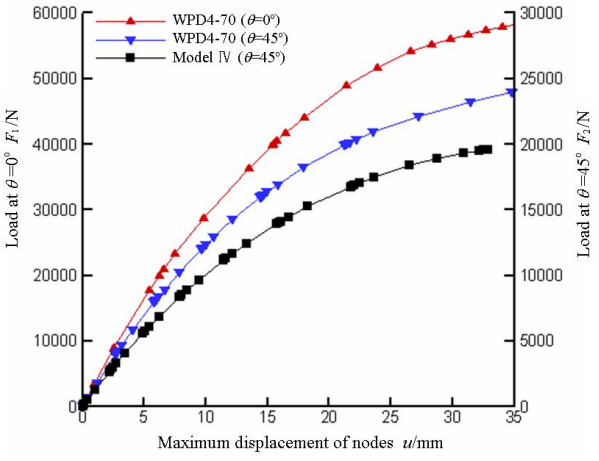

Fig. 15. Relation curve about the load and the maximum displacement of nodes

As can be seen, the strength characteristics of WPD4-70 are improved compared with model Ⅳ, and that at θ=45° are critical to ensure the safety of its wheeled function. The large elastic deformation of WPD4-70 has been seriously affected the security and stableness when it reaches the critical buckling value, shown in Fig. 16. Therefore, 1% of

WPD4-70's diameter is defined as the maximum allowable deformation, and the corresponding load capacity (3 975 N) is the maximum allowable load, which can ensure the driving safety of the multi-moving state AUV.

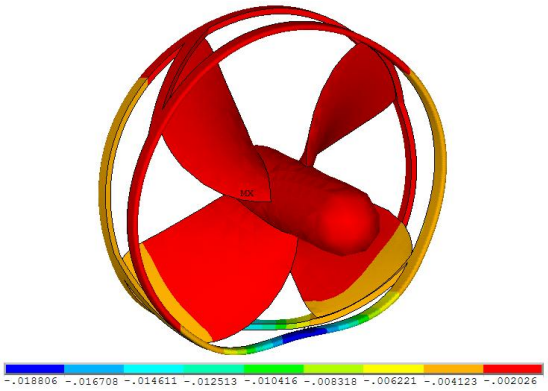

Fig. 16. Nodes' displacement of WPD4-70 at the critical buckling (θ=45°) (mm)

5.2 New wheel propeller modal analysis

Modal analysis that used to determine the vibration characteristics of the structure is the basis for dynamic analysis. According to vibration theory and finite element method, the free vibration characteristics (natural frequencies and mode shapes) of WPD4-70 are obtained by solving the free vibration equations.

The first five natural frequencies of model Ⅳ and WPD4-70 are computed using Block-lanczos method, shown in Table 2, all natural frequencies of WPD4-70 are less than that of model Ⅳ, which shows that the ability of its vibration insulation in the driving state is enhanced.

Table 2. Natural frequencies of model Ⅳ Hz

Model	First order	Second order	Third order	Fourth order	Fifth order
Model Ⅳ	1006.36	1754.87	1888.20	1957.13	2021.90
WPD4-70	941.30	1593.23	1795.50	1924.37	1970.20

6 Conclusions

(1) A new wheel propeller is designed through analyzing the mechanical characteristics of the ducted propeller and the CLT propeller, which breaks through the traditional design methods and realizes the agile maneuverability of the multi-moving state AUV.

(2) The CFD method is used to simulate numerically different propellers' open-water performance by using the RANS equations and RSM based on sub-domains hybrid meshes, which guides to design the wheel propeller. The computational data of the open-water performance agree well with the experimental data. It shows that the numerical method has good accuracy in the prediction of propellers' open-water performance.

(3) Finite element method is used to make nonlinear buckling analysis, and the maximum allowable load is obtained on the premise of ensuring the security and stability of the AUV when it is moving on the ground. Then the natural frequencies and mode shapes of WPD4-70 are computed through the modal analysis, which lay a foundation for the structural design and dynamic analysis of the multi-moving state AUV.

(4) The WPD4-70 designed in this paper has better open-water performance and strength characteristics, which meet the requirements of navigation and wheeled function, so the multi-moving state AUV can achieve more movements such as vectored navigation, submarine landing and submarine driving.

References

[1] HOU W. *System control and experiments on autonomous underwater vehicle with capabilities of landing and sitting-bottom* [D]. Tianjin: Tianjin University, 2006.

[2] PAN C Y, WEN X S. Research on Transmission principle and kinematic analysis for involute spherical gear[J]. *Chinese Journal of Mechanical Engineering*, 2005, 41(5): 1–9.

[3] GAO F D, PAN C Y, CAI W S, et al. Numerical analysis and validation of propeller open-water performance based on CFD[J]. *Chinese Journal of Mechanical Engineering*, 2010, 46(8): 133–139.

[4] KERWIN J E, TAYLOR T E, BLACK S D, et al. A coupled lifting-surface analysis technique for marine propulsors in steady flow[C]//*Proceedings of the Propellers/Shafting'97 Symposium*, September 23–24, 1997, Virginia Beach, VA, USA: SNAME, 1997: 1–15.

[5] DONG S T, TANG D H, ZHOU W X. Panel method of CSSRC for propeller in steady flows[J]. *Journal of Ship Mechanics*, 2005, 9(5): 46–60.

[6] RHEE S H, JOSHI S. CFD validation for a marine propeller using an unstructured mesh based RANS method[C]//*Proceedings of FEDSM'03*, the 4th ASME- JSME Fluids Engineering, July 6–11, 2003, Honolulu, Hawaii: ASME, 2003: 1–7.

[7] GONG L, YAO Z, WU M. Numerical analysis for hydraulic characteristics of marine propeller under reverse bent and twist[J]. *J. University of Shanghai for Science and Technology*, 2007, 29(1): 65–69.

[8] TAHARA Y, HIMENO Y. Applications of isotropic and anisotropic turbulence models to ship flow computation[J]. *Kansai Soc. N. A. , Japan*, 1996, 225: 75–91.

[9] HUGHES M J, KINNAS S A, KERWIN J E. Experimental validation of a ducted propeller analysis method[J]. *Journal of Fluids Engineering*, 1992, 114(6): 214–219.

[10] FORNELLS R G, GOMEZ G P. Full-scale results of the first TVP propeller[J]. *The Naval Architect*, 1983, 11: 291–295.

[11] ANDERSEN P, SCHWANECKE H. Design and model test of tip fin propellers[J]. *Transactions of the Royal Institution of Naval Architects*, 1992, 134: 315–320.

[12] CUI C G, SHI N J. An investigation on the performance of a screw with end plates at blade tips[J]. *J. Huazhong Univ. of Sci. &Tech*, 1991, 19(8): 117–120.

[13] SHENG Z B, YANG J S, CAI Y Y. *Experimental atlas of Chinese ship propellers*[M]. Shanghai: Ship Building of China Press, 1983.

[14] JIANG F C, ZHU C M, XUE J S. Non-linear analysis of buckling carrying capacity for corroded reinforcing bars based on ANSYS[J]. *Journal of Tongji University*, 2008, 36(8): 1 045–1 049.

Biographical notes

GAO Fudong, born in 1982, is currently a PhD candidate at *College of Mechatronic Engineering and Automation, National*

University of Defense Technology, China. He received his bachelor degree and master degree in 2005 and 2007, respectively from *National University of Defense Technology, China*. His research interests include computational fluid dynamics, design and performance prediction of submerged weapons.
Tel: +86-731-84574932; E-mail: gaofudong2005@163.com

PAN Cunyun, born in 1955, is currently a professor at *National University of Defense Technology, China*. His research interests include mechachonics engineering and robotics and ocean engineering.
Tel: +86-731-84576481; E-mail: pancunyun@sina.com

XU Haijun, born in 1981, is currently a PhD candidate at *College of Mechatronic Engineering and Automation, National University of Defense Technology, China*.
Tel: +86-731-84574932; E-mail: xuhaijun-1999@163.com

ZUO Xiaobo, born in 1983, is currently a PhD candidate at *College of Mechatronic Engineering and Automation, National University of Defense Technology, China*.
Tel: +86-731-84574938; E-mail: zuoxbgfkd@163.com